Advanced Materials Research Vols. 89-91 (2010) pp 85-90
© (2010) Trans Tech Publications, Switzerland
doi:10.4028/www.scientific.net/AMR.89-91.85

Analysis of the Homogeneity of Particle Refinement in Friction Stir Processing Al-Si alloys

Chun Y. Chan[1a], Philip B Prangnell[1b] and Simon J Barnes[2c]

[1]Materials Science Centre, School of Materials, The University of Manchester, Grosvenor Street, Manchester, M1 7HS, UK. [2] SB2 Metallurgical Services, Unit 37, SFWBC, Great Central Way, Rugby, CV21 3XH, UK

[a]c.y.chan@student.manchester.ac.uk, [b]philip.prangnell@manchester.ac.uk, [c]Simon.Barnes-2@manchester.ac.uk

Keywords: Friction stir processing; FSP; Al-Si, particle refinement.

Abstract. Friction Stir Processing (FSP) has potential for locally enhancing the properties of Al-Si alloy castings, for demanding applications within the automotive industry, by greatly refining the second phase particle size. In the present study, the homogeneity of particle refinement and second phase spatial distribution within the process zone, as well as the relationship to the processing parameters, were investigated in a gravity die cast Al-Si LM24/A380 alloy, subjected to a range of FSP conditions. Detailed image analysis and the dirichlet tessellation method were used to quantify particle clustering. 'Stop-action' experiments were also used to study the process of particle break up, by following the behaviour through the deformation zone surrounding the tool.

Introduction

Al-Si alloys are widely used in automotive engine applications because of their low cost and density, and high temperature capability, combined with excellent castability. However, in order to increase engine efficiency, there are demands for ever more severe operating conditions, which will require improvements to the performance of current materials. Friction Stir Processing (FSP) [1-11] is a variant of the Friction Stir Welding (FSW) process, where the intense deformation generated by traversing a rotating welding tool, has been exploited as a technique of microstructural refinement in a range of materials [1]. Investigations into the use of FSP have shown that it can lead to a dramatic reduction in grain size and a high level of second phase particle refinement [1,3,4]. By refining the microstructure of cast Al-Si alloys, the high temperature mechanical performance and, in particular, fatigue properties should be improved [1,4,5]. The technique thus has potential for locally enhancing the microstructure in highly stressed areas of cast Al-Si engine components, such as piston crowns and cylinder heads.

Previous investigations into the effect of FSP on Al-Si casting alloys have shown that high levels of microstructural refinement can be achieved, with the size of the Si particles being reduced to less than 3 μm in sand castings, or even finer, to less than 1 μm in chemically modified castings containing fibrous eutectic Si [6-10]. At the same time, there is a reduction in porosity and the grain size can be reduced to below 5 μm. By subjecting Al-Si alloys to FSP, the tensile and fatigue properties have also been found to improve [6-9]. Some researchers have reported the effect of the processing parameters on the level of refinement that can be achieved (e.g. [1,9-11]). Observations to date include an increase in homogeneity [10] and a slight reduction in particle size with tool RPM [11]. However, in general these investigations have not quantified the homogeneity of the distribution of Si particles and other intermetallic phases throughout the processed zone (PZ).

In the present study the microstructure of a hypo-eutectic gravity die cast Al-Si A380 alloy, subjected to a range of FSP conditions, was investigated. Image analysis of particle size distributions and the Dirichlet Tessellation method were used to quantify the level of particle refinement and the homogeneity of the second phase spatial distribution, as a function of location within the process

zone, as well as the relationship to the processing conditions (rotation speed and transverse speed). 'Stop-action' experiments were also conducted to study the particle break up, by examining the refinement behaviour through the deformation zone surrounding the tool.

Experimental

A hypo-eutectic LM24/A380 Al-Si alloy (Al-8.9Si wt%), gravity cast in a steel mould, as 296 mm x 210 mm x 26mm plates, was used in the FSP experiments. Prior to FSP, the plate were milled back 2 mm to generate flat surfaces for processing. Friction stir processing was carried out using a CS Powerstir Friction Stir Welding machine and a H13 steel tool, with a 20 mm diameter shoulder and threaded, tapered, tri-flat pin 5.8 mm in length. To investigate the effect of the FSP parameters, the cast slabs were first processed at a fixed transverse speed of 200 mm/min, using a range of tool rotation speeds from 300 rpm to 900 rpm, increasing in increments of 200 rpm. The effect of travel speed was also studied from 100 to 400 mm/min using a matrix of rotation speeds. The plate temperature was monitored in all the tests with embedded thermocouples placed close to the tool. Processing conditions were also selected that produced similar peak temperatures in the process zone, while changing the travel speed.

To further investigate the mechanism of particle breakup, stop-action samples were produced using the conditions of 200 mm min^{-1} and 500 rpm. This involved immediately stopping the FSW machine with the pin still embedded within the plate. The processed zone was then carefully cut out of the plate and the sample sectioned with the tool in-situ. The particle's size distributions, average size, and spatial distribution were quantified by optical microscopy using ImagePro analysis software. Particle sizes are defined by the equivalent circular diameter (ECD). The Dirichlet Tessellation method was used to characterise the particle's spatial distribution [12].

Results and Discussion

Particle Size Distributions within the Process Zone. The parent cast alloy is shown in Fig. 1(a) and contained eutectic Si with a coarse flake morphology, but also a significant volume fraction of finer irregular eutectic α -AlFeMnSi and Al_2Cu. The initial second phase average particle size was 6.2 μm (ECD) with distinctly different morphologies for the different phases. After FSP the microstructure of the cast Al-Si alloy was greatly refined within the processed zone (PZ) (e.g. Fig. 1(b), (c)). The large high aspect ratio plate like eutectic Si particles and other intermetallic phases were broken up into low aspect ratio fine angular particles with an average size in the range of 2 to 3 μm. However, the particle size distributions had a large tail (see Fig. 1(d)) and, although it was impossible to accurately separate the individual phases by optical image analysis, the larger particles tended to be fragments from the coarser Si eutectic flakes. Voids which existed within the original cast material were also removed by FSP. For all of the welding conditions the mean local particle size was evaluated across the PZ, at half the tool depth, and down the centre of the PZ, while the average particle sizes taken from all these readings are plotted against rotation speed (Fig. 2(d)).

From Fig. 2 it can be seen that the particle sizes are not very sensitive to the welding conditions varying little with tool rpm or travel speed. However, they are not uniform across the PZ, increasing towards the retreating side and reducing from top to bottom down the centre line. The reduction in particle size towards the bottom of the PZ is most likely due to the thermal gradient though the plate. The bottom, of what is effectively a 6 mm deep partial penetration weld, was determined to be ~ 100 °C colder than the top, due to the heat sink effect of the 25 mm thick plate and the higher heat input from the tool shoulder. The difference in refinement across the PZ will be discussed below when the stop-action sample is considered. Furthermore, for this welding travel speed (200 mm/min), taken overall (Fig. 2(d)), the data suggests that there is a small increase in particle size when averaged over the whole PZ with tool RPM. This contradicts the findings of Ma et al. [11] who reported a slight

reduction in particle size with higher tool rotation speeds. This again suggests that the temperatures reached near the tool dominate the average level of particle refinement seen in the PZ.

The tool travel speed was also varied from 100 to 400 mm/min with the rotation speed selected to try to keep the maximum temperatures in the weld zone relatively constant, on the basis of thermocouple measurements. This data is presented in Fig. 2(c). While it is difficult to be sure of exactly maintaining a constant temperature, as it is not possible to measure close enough to the tool interface, this data shows little variation in average particle size with increasing travel speed.

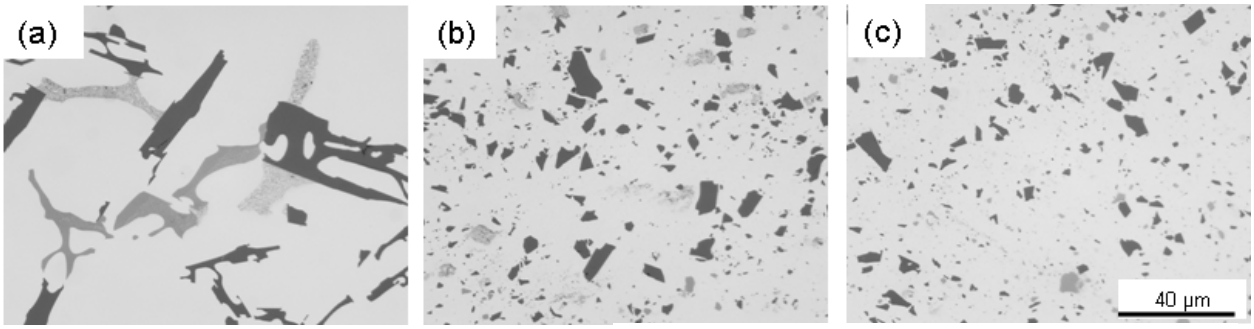

Fig. 1: The cast starting material (a) showing coarse flake eutectic Si (dark), α AlFeMnSi (medium grey), and Al_2Cu (light grey) phases and from the centre of the PZ after; FSP 200 mm min^{-1} at ; (b) 300 RPM and (c) 900 RPM. In (d) a typical particle size distribution is shown from the 300 RPM sample.

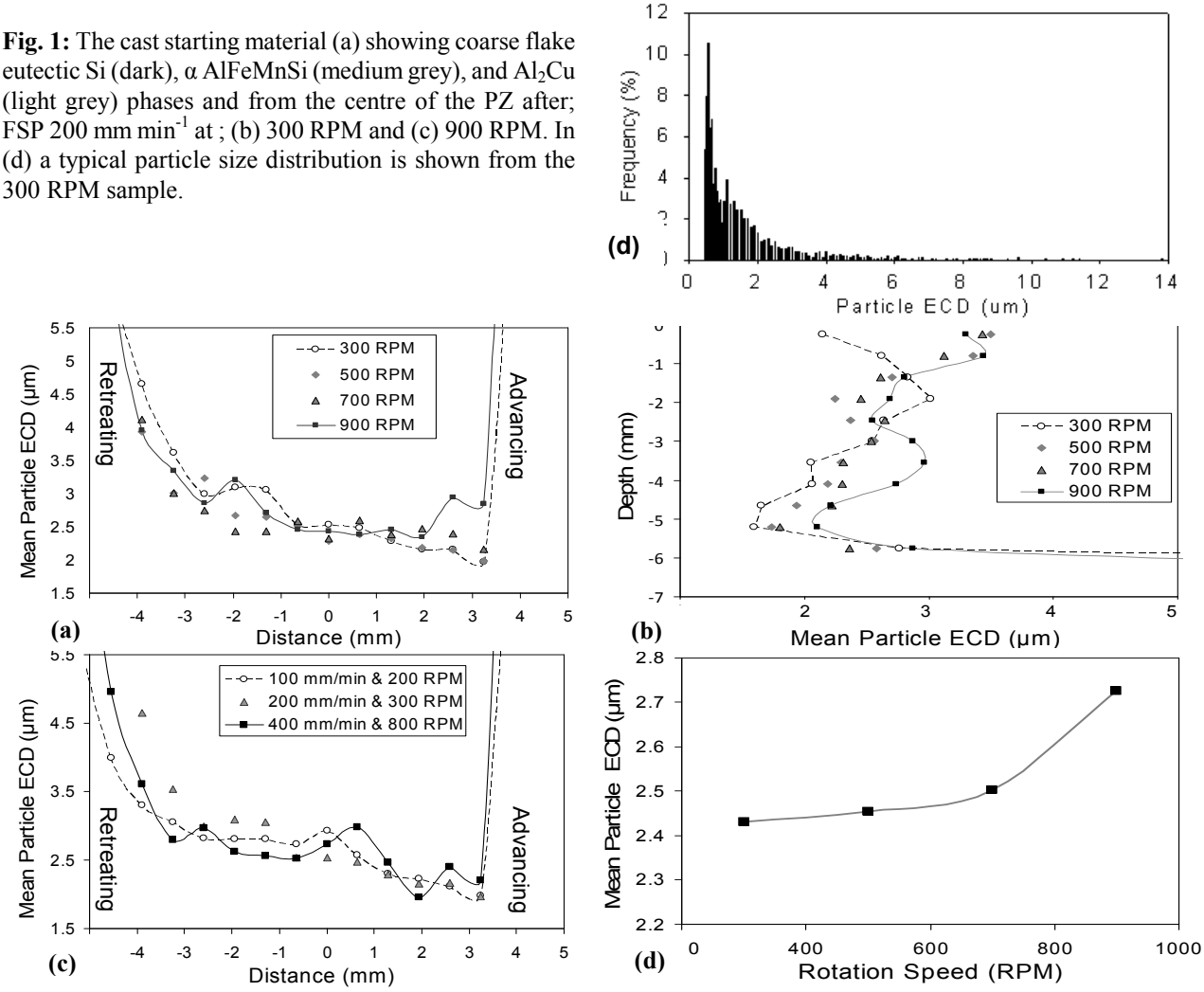

Fig. 2: Average particle sizes (ECD) measured (a) across and (b) down the centre of the PZ, after FSP at 200 mm min^{-1} with a range of ration speeds, and (c) across the PZ for a range of travel speeds, with the rotation speed selected in an attempt to maintain similar temperatures within the deformation zone. In (d) the particle size averaged across the entire PZ is plotted against rotation speed.

Homogeneity of Particle Distribution. A tessellation technique was used to investigate the homogeneity of the particle's spatial distribution within the process zone, by expanding each particle until impingement [12]. Analysis of the resulting cell distributions could then be used to quantify the

homogeneity of the particle's spatial distribution, as function of their position and the welding conditions. This data is summarized in Fig. 3(a), which gives the standard deviation of the cell area distributions across the process zone. Examples of cells constructed from images taken at 3.5 mm from the centre line on the retreating side, where the particles were coarser and less homogeneously distributed (see inserts in Fig 4) are shown in Fig. 3(b). From this data it is clear that, as well as the average particle size increasing, the degree of clustering, or inhomogeneity in spatial distribution also rises across the PZ from the advancing to the retreating side. However, this behaviour is less pronounced when a higher rotation speed is used and the particle's spacing becomes more homogeneous across the processed zone, resulting in a reduced gradient in the data in Fig. 3(a). Ma et al. have also reported more uniform particle distributions at higher rotation speeds [11].

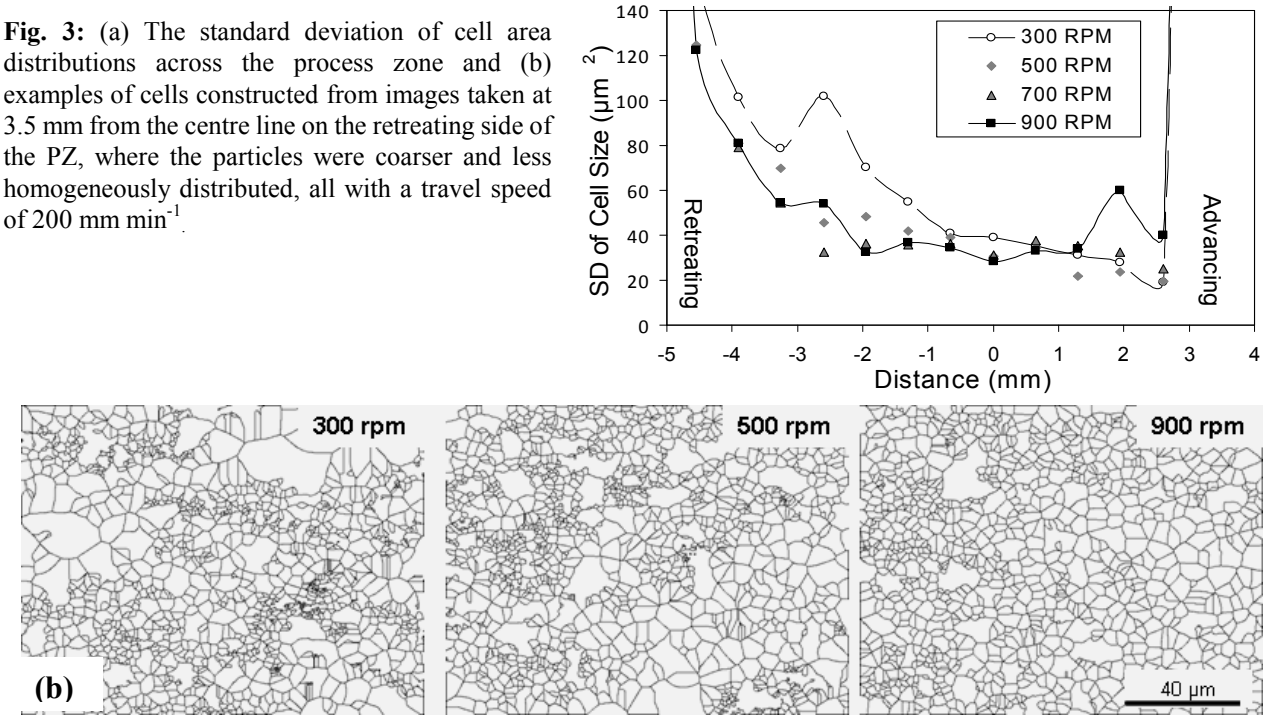

Fig. 3: (a) The standard deviation of cell area distributions across the process zone and (b) examples of cells constructed from images taken at 3.5 mm from the centre line on the retreating side of the PZ, where the particles were coarser and less homogeneously distributed, all with a travel speed of 200 mm min^{-1}.

Stop Action Sample. The stop action processed sample was sectioned in plan view at a depth of 4.2 mm below the plate surface, where the material flow is dominated by the pin. Fig. 4 shows the microstructure that develops around the pin as it interacts with the material. Unfortunately, some defects have developed for this processing condition, associated with the flats on the pin design. Nevertheless, this specimen shows some very interesting features. Firstly, the direction of flow can be seen to always be in the direction of tool rotation, even on the advancing side. Secondly, the deformation zone is very narrow and closely confined to the tool surface, being < 100 μm wide on the advancing side, but increasing to just less than 1 mm on the retreating side. Thirdly, particle break up occurs within the shear layer, most effectively in material originating from ahead of the tool on the advancing side, which experiences the highest strain rate and strain, before being deposited behind the tool in roughly the same position. In comparison, material on the retreating side experiences a lower strain rate and strain and is displaced least by the tool [13]. This asymmetric flow behaviour has been modelled by several models for FSW and the strain rate of material entering the shear layer on the advancing side is generally predicted to be of the order of 10-100 times higher than on the retreating side (e.g. [14,15]). Particle break up occurs progressively as material enters the shear zone, due to the intense shear strain, with few particles actually interacting directly with the tool surface. However, it is difficult to ascertain the influence of the tool surface features with this one snap shot. Particle break up thus largely occurs by load transfer from the soft plastically deforming matrix to the hard non-deformable second phases. The load on the particles causing their fracture will therefore be a strong function of the matrix flow stress, which is controlled by the Zener Holloman parameter and will reduce at higher temperatures and lower strain rates [16]. Given the limited range of particle sizes

with processing parameters, at the enormous strain levels seen in FSP it is likely, the refined particles are approaching a lower size limit, which is dictated by their minimum dimension and, or their original defect density, caused by branching, twinning, or other stress concentrations arising from when they first formed as irregular eutectics.

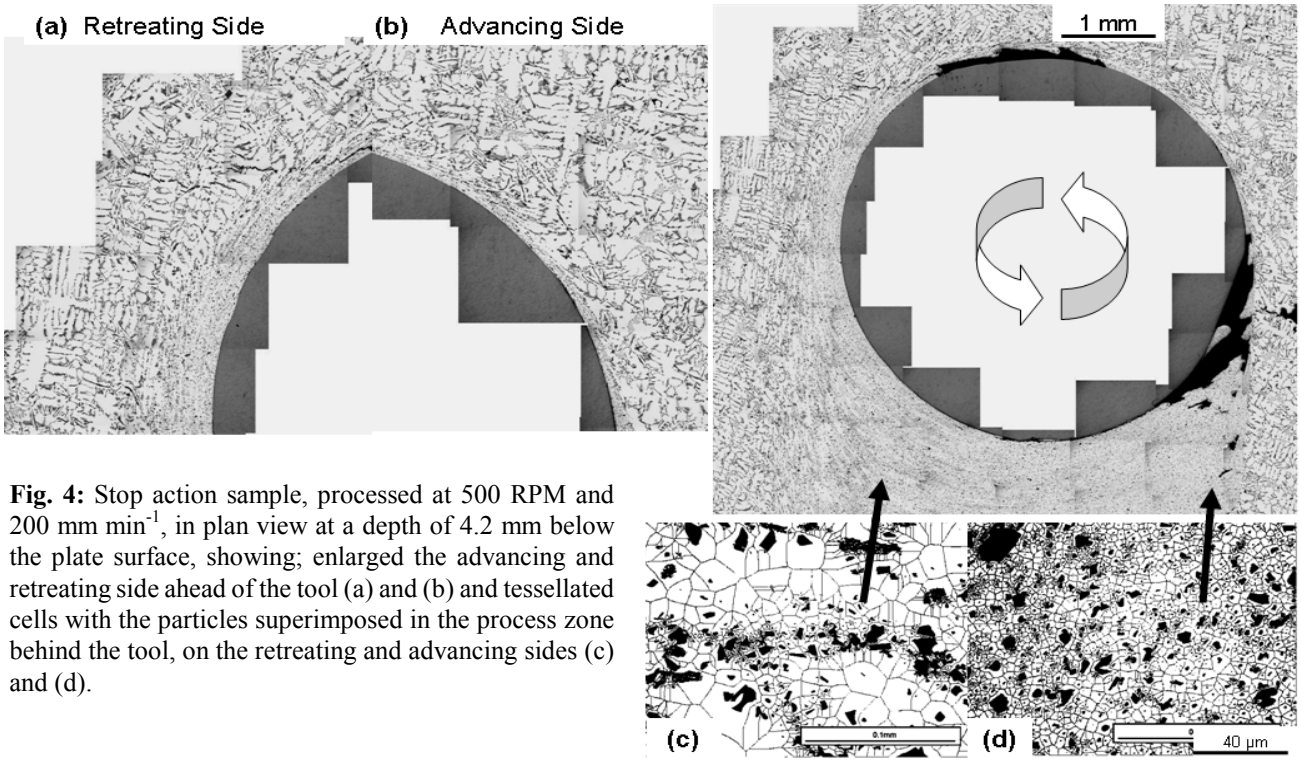

Fig. 4: Stop action sample, processed at 500 RPM and 200 mm min^{-1}, in plan view at a depth of 4.2 mm below the plate surface, showing; enlarged the advancing and retreating side ahead of the tool (a) and (b) and tessellated cells with the particles superimposed in the process zone behind the tool, on the retreating and advancing sides (c) and (d).

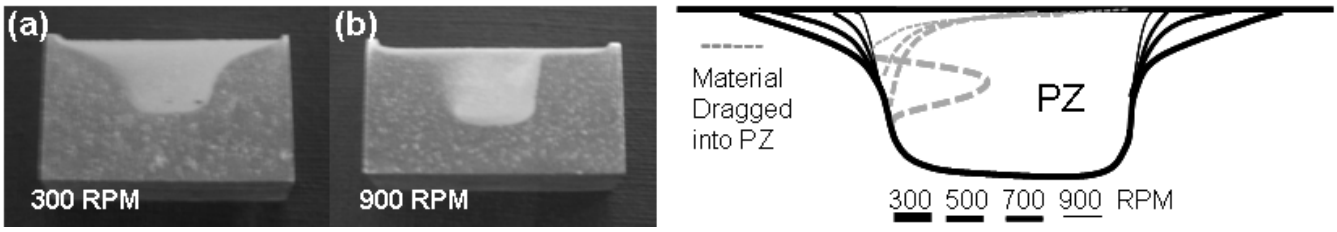

Fig. 5: Profiles of the PZ shown in example macrographs (a) and (b) and mapped in (c) following FSP at 200 mm min^{-1} with increasing tool RPM.

A further interesting point is to understand why the particle size and spatial distribution becomes more uniform across the PZ when a higher rotation speed is used. Part of the explanation for this behaviour is the change in PZ size and material flow as the rate of tool rotation is increased. The change in PZ cross-section with rotation speed is shown in Fig. 5, where it can be seen that the deformation zone is more asymmetric and wider at low RPM and becomes tighter to the tool profile as the tool rotation rate increases. At low rotation rates the shear zone is wider and the material deforms at a greater distance from the tool surfaces, with the shoulder having a bigger influence. This actually displaces the nugget (Fig. 5(c)), with less refined material being swept in from the side by the back of the shoulder behind the pin as the tool travels forwards. At high speeds the shoulder affects the material to a much shallower depth and the PZ profile on the retreating side becomes much closer to the tool. This behaviour has been seen previously in FSW, where the material flow stress rapidly decreases at high temperatures as the melting point is approached, leading to a reduction in width of the shear zone [15]. This reduction in shear zone width is most noticeable on the retreating side of the tool and will lead to a greater symmetry of deformation between material that ends up at either the advancing or retreating side of the tool behind the pin. Furthermore, a higher rotation rate leads to a smaller pitch, which reduces from 0.7 mm/rev to 0.2 mm/rev with the tool RPM increasing from 300 to 900. This means a smaller volume of material needs to be displaced per revolution. It is also known

that the flow driven by the pin is cyclic, with a periodic change in strain rate, associated with non-concentricity of the tool, and features such as flats or threads [14]. With a similar tri-flat tool it has been shown that texture bands in the process zone repeat the same distance as the pitch, equivalent to a full tool rotation, as well as the pitch/3, caused by the three flats on the tool [17]. This intermittent flow has been shown to cause particle banding in other alloys [18] and the frequency will become much finer at higher rotation speeds increasing the homogeneity of the particle dispersion.

Conclusions

In the present study the homogeneity of particle refinement and second phase spatial distribution was investigated, within the process zone developed during FSP, in a gravity die cast A380 Al-Si alloy. The high level of refinement that can be achieved by FSP resulted in an average particle size of 2 to 3 μm within the processed zone, which was relatively insensitive to the processing conditions. However, there was a tendency for the average particle size to increase slightly with tool rotation speed, as well as to reduce from top to bottom, and increase across the centre of the PZ, from the advancing to retreating side. Providing a sufficient strain is reached, the dominating factor controlling the particle size appears to be the temperature and corresponding matrix flow stress within the shear layer at the tool surface. On the retreating side of the PZ the wider deformation layer and lower strain rate and strain leads to a lower level of refinement. The homogeneity of the particle dispersion also reduced from the advancing to the retreating side of the PZ and increased with rotation speed. This behaviour has been linked to a decrease in pitch and a reduction in width of the shear zone, which becomes more symmetric and shrinks closer to the tool profile at high rotation speeds.

Acknowledgements

The leading authors would like to thank LATEST, the University of Manchester EPSRC Light alloys Portfolio Partnership (EP/D029201/1) for funding this research.

References

[1] R.Mishra, in*: Friction Stir Welding and Processing*, edited by R.S. Mishra, M.W. Mahoney: ASM (2007), p. 309.
[2] C.G. Rhodes, M.W. Mahoney, W.H. Bingel, M. Calabrese: Scripta Mater. 48 (2003), p. 1451.
[3] R.S. Mishra, Z.Y. Ma, I. Charit: Mater. Sci. Eng. 341A (2003), p. 307.
[4] Z.Y. Ma, A.L. Pilchak, M.C. Juhas, J.C. Williams: Scripta Mater. 58 (2008), p. 361.
[5] L.B. Johannes, I. Charit, R.S. Mishra, R. Verma: Mater. Sci. Eng. 464A (2007), p. 351.
[6] W.B. Lee, Y.M. Yeon, S.B. Jung: Mater. Sci. Eng. 355A (2003), p. 154.
[7] S.R. Sharma, Z.Y. Ma, R.S. Mishra: Scripta Mater. 51 (2004), p. 237.
[8] M.L. Santella, T. Engstrom, D. Storjohann: Scripta Mater. 53 (2005), p. 201.
[9] Z.Y. Ma, S.R. Sharma, R.S. Mishra : Scripta Mater. 54 (2006), p. 1623.
[10] Z.Y. Ma, S.R. Sharma, R.S. Mishra: Mater. Sci. Eng. 433A (2006), p. 269.
[11] Z.Y. Ma, S.R. Sharma, R.S. Mishra: Metall. Mater. Trans. 37A (2006), p. 3323.
[12] P.B. Prangnell, S.J Barnes, S.M. Roberts, P.J. Withers: Mat. Sci. Eng. A220 (1996), p. 41.
[13] A.P.Reynolds: Sci. Technol. Weld. Joining 5 (200), p. 120.
[14] P.A. Colegrove, H.R. Shercliff: Sci. Technol. Weld. Joining 9 (2004), p. 483.
[15] P.A. Colegrove, H.R. Shercliff, R. Zettler: Sci. Technol. Weld. Joining 12 (2007), p. 284.
[16] S.M. Roberts, P.J. Withers, S.J. Barnes and P.B. Prangnell, in: *the Numerical Predictions of Deformation Processes and the Behaviour of Real Materials*, 15th Risø Int. Symp, edited by. S.I. Andersen, et al., Roskilde, DK, (1994), p. 505.
[17] P.B. Prangnell, C.P. Heason: Acta Mater. 53 (2005), p. 3179.
[18] A.F. Norman, I. Brough, P.B. Prangnell: Mat. Sci. Forum Vol. 331-337 (2000), p. 1713.